

Nonlinear refractive indices of nonlinear liquids: wavelength dependence and influence of retarded response

Stefan Kedenburg · Andy Steinmann ·
Robin Hegenbarth · Tobias Steinle ·
Harald Giessen

Received: 29 November 2013 / Accepted: 2 April 2014 / Published online: 27 April 2014
© Springer-Verlag Berlin Heidelberg 2014

Abstract We use liquid-filled capillary fibers with different core diameters to precisely characterize the nonlinear refractive index of the highly nonlinear liquids carbon disulfide, nitrobenzene, and toluene. We present measurements with two different femtosecond pump sources at wavelengths of 1032 and 1560 nm. The large nonlinearity of the liquids results from the retarded nonlinear optical response of the liquid molecules which includes a strong non-instantaneous contribution due to molecular reorientation. The nonlinear refractive index of the liquids is determined by fitting numerical simulations based on solving the generalized nonlinear Schrödinger equation including retarded response to the measured broadened output spectra. Our work is important for the novel field of near- and mid-IR supercontinuum generation in liquid-core optical fibers.

1 Introduction

Highly nonlinear liquids offer striking possibilities in the field of optics because they are especially suited for generating supercontinuum due to their relatively high nonlinear refractive indices when compared to solids (up to 100 times larger compared to fused silica [1]).

Broad mid-infrared supercontinuum sources are very interesting and sought after in research because they can excite vibrational absorption bands in the molecular fingerprint region (2.5–25 μm), which makes it possible to specifically identify molecules and functional groups [2].

Furthermore, for the generation of nonlinear optical responses, very high intensities are needed. Optical fibers, with their small cross-section area, can provide the required intensities over a long interaction length. However, due to the small nonlinear refractive index of fused silica, special non-silica fibers such as ZBLAN [3] or chalcogenide-based fibers [4] have been developed with larger transmission ranges and improved nonlinear optical properties, but they are limited in functionality and flexibility.

To combine the advantages of high nonlinearities of liquids and high peak intensities in fibers, selectively liquid-filled photonic crystal fibers [5–7] and integrated liquid-core optical fibers [8–10] have come into focus. The advantage of this combination is that the dispersion properties can be tailored accordingly, e.g., by changing the core radius, using mixtures of different liquids, or changing their temperature and hence $n(T)$ [11]. A further benefit is that some highly nonlinear liquids possess a very broad transparently range in the mid-infrared region [12] which is crucial for extending supercontinua far into this spectral region. The highly nonlinear properties of the liquids allow for reduction in the required intensities significantly, which makes liquid-filled fibers also accessible for cheap, compact pump lasers.

Moreover, the characteristics of self-phase modulation can be studied in such liquid-filled capillary devices [13], which makes it possible to precisely measure nonlinear refractive index data of the core liquids. In the literature, only broadly scattered values are reported, which are measured with sub-nanosecond pulses in the near-infrared spectral region [14, 15]. Nowadays, compact fs laser become more abundant [16].

Therefore, in this paper, we precisely measure the nonlinear refractive index n_{21} of carbon disulfide (CS_2), nitrobenzene ($\text{C}_6\text{H}_5\text{NO}_2$), and toluene (C_7H_8) with

S. Kedenburg (✉) · A. Steinmann · R. Hegenbarth ·
T. Steinle · H. Giessen
4th Physics Institute and Research Center SCOPE,
University of Stuttgart, 70550 Stuttgart, Germany
e-mail: s.kedenburg@pi4.uni-stuttgart.de

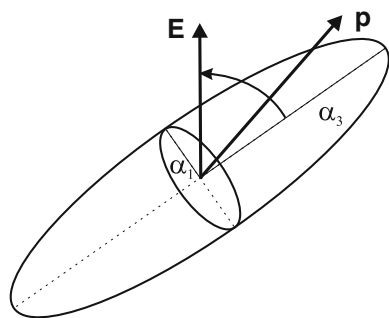


Fig. 1 A cigar-shaped molecule, such as CS_2 has a larger polarizability α_3 along the symmetry axis, as perpendicular to it ($\alpha_3 > \alpha_1$). The induced dipole moment \mathbf{p} thus will not be parallel to \mathbf{E} but experience a torque that tries to align the molecule along the applied electric field. The associated change of refractive index is proportional to $|\mathbf{E}|^2$ [18]

femtosecond pulses at two particular wavelengths of 1032 and 1560 nm and determine the characteristic delayed molecular contribution f_m attributed to molecular reorientation [17], among other mechanism. The reason for the high nonlinearity of liquids is molecular reorientation. It originates from the tendency of anisotropic molecules to become aligned in the electric field of an applied optical wave. When a light field \mathbf{E} hits a dipole \mathbf{p} which is not aligned along \mathbf{E} , it tries to reorient it along \mathbf{E} counteracting the thermal agitation as depicted in Fig. 1. This leads to a modified value of the refractive index because the average polarizability has been changed by the molecular alignment. This effect is proportional to $|\mathbf{E}|^2$ and hence nonlinear in the applied field [18].

2 Measurement Techniques

An easy and precise method to measure the nonlinear refractive index n_{21} is provided by the evaluation of the broadened frequency spectrum. The broadening results from a combination of self-phase modulation and especially in liquids from an additional non-negligible retarded response effect. The nonlinear material response function $R(t)$ includes an instantaneous electronic as well as a slower nuclear contribution. The functional form is given by

$$R(t) = (1 - f_m)\delta(t) + f_m h_m(t), \quad (1)$$

with f_m being the fraction and h_m representing the delayed response. The fast electronic contribution can be simply described by a Dirac delta function $\delta(t)$. Despite the instantaneous Kerr electronic nonlinearity [(first term of Eq. (1)), the so-called reorientational nonlinearity [19] [(second term of Eq. (1))] dominates in liquids for ps and sub-ps pulses, f_m becomes as high as 0.90 in CS_2 . The alignment of the initially thermally orientated liquid

molecules with a permanent anisotropic molecular polarizability by the incoming light explains the high nonlinearity of some liquids in comparison with solids, where only the electrons are contributing [17].

Depending on the pulse duration and its agreement to the reaction time of the liquid molecules, the strength of the dominating reorientational contribution changes. Hence, for pulses much shorter than the relaxation time of the liquids, which lies in the ps-range [18, 19], the effect of the reorientational nonlinearity will be small, since the response does not have sufficient time to accumulate. Therefore, the nonlinear refractive index $n_{21}(\lambda, T_0)$ strongly depends, beside the wavelength λ , also on the pulse duration T_0 [6], especially in the investigated transition regime of subpicosecond pulses.

The reorientational response function of the highly nonlinear and mostly investigated liquid CS_2 is described in the following in more detail. However, its functional behavior can also be transferred to other liquids.

In the relaxation dynamics of CS_2 three distinct temporal responses of the nuclear contribution play a role [20], which are combined in the reorientational response function $h_m(t)$. The time constant for the slowly exponential decaying dynamics in CS_2 is 1.68 ps and over 10 times higher compared to the Raman response of fused silica [21]. The dynamics of molecular motion in liquids can be measured by the time-resolved optical Kerr effect where the excited molecules are sensed by a few femtosecond long probe pulse. At long timescales (few picoseconds), the motion is described by diffusive reorientations, whereas for shorter times (100 fs–1 ps), the dynamics consist of complex intermolecular motions. The latter dynamics can be described by an intermediate response that is associated with the interaction-induced distortion of the molecular polarizability and by a rapidly damped oscillatory behavior assigned to molecular librational motion [17]. The three nuclear responses are modeled by [20]

$$h_m(t) = A_1 e^{-t/t_{\text{diff}}} (1 - e^{-t/t_{\text{rise},1}}) + A_2 e^{-t/t_{\text{int}}} (1 - e^{-t/t_{\text{rise},1}}) + A_3 e^{-t^2/(2t_{\text{fast}}^2)} \sin(t/t_{\text{rise},2}), \quad (2)$$

with a diffusive (t_{diff}), an intermediate (t_{int}), and a librational (t_{fast}) relaxation process. To account for the inertial effects, a rise time (t_{rise}) is included which should be similar for all of the non-instantaneous nuclear responses [17]. The effects of the individual components and the complete reorientational response function of CS_2 are shown in Fig. 2.

The reorientational response function in liquids is non-oscillating and only slowly approaches zero, in contrast to the delayed Raman response in glass which is characterized by intramolecular vibrations.

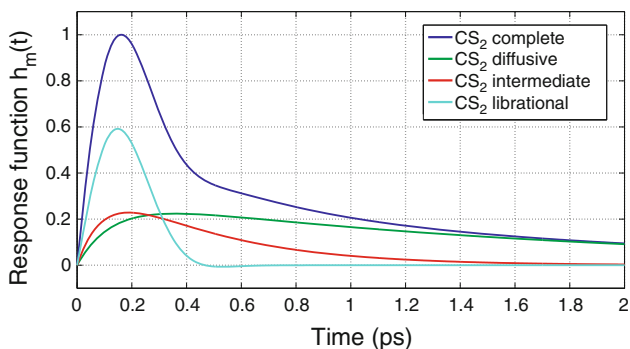


Fig. 2 Contributions of the individual components of the reorientational response functions $h_m(t)$ for CS₂ (green, red, and turquoise curve) [20]. The complete response function (blue curve) shows no oscillations but a slow decaying trend in comparison with the Raman response of fused silica [21]

For the response function $h_m(t)$ of toluene, the same functional form as for carbon disulfide in Eq. (2) has been used. For nitrobenzene, the best fitting results are obtained if the third term of Eq. (2) is substituted by the functional form of the first term. The given coefficients in Table 1 are either directly taken from the corresponding references or are the results of a fitting procedure using the data plotted in the corresponding references, whereas the time constants are adopted, respectively [20, 22–24]. In addition, the coefficients were normalized according to $\int h_m(t)dt = 1$.

The reorientational response functions $h_m(t)$ for all investigated liquids are shown in Fig. 3.

A consequence of taking not only the instantaneous response but also the delayed reorientational contribution into account, which is mainly responsible for the high nonlinearity, is that the measured output spectrum behind the liquid-filled capillaries can only be evaluated numerically. This has been realized by solving the generalized nonlinear Schrödinger equation (NLSE) using a split-step Fourier method [25] instead of the analytical expression suggested in the paper of Huy and co-workers [13]. The generalized NLSE has been proven to accurately describe the propagation of ultrashort laser pulses in optical fibers [26]. Nevertheless, the analytical model has served as a test reference for the numerical model when evaluating the spectra of a fused silica fiber, where the retarded (Raman) response plays a minor role and the usual self-phase modulation is the dominating nonlinear effect (see Fig. 4).

Also the advantage of fitting the whole transmitted intensity spectrum remains the same. The method enables a clean and exploitable measurement of the nonlinearity of the liquids at relatively low power values so that the additional and superimposed effect of the Raman nonlinearity can be neglected in our case [6, 19]. The pulses used by us do not have the necessary bandwidth to excite those Raman-active modes in the molecule. The only drawback

Table 1 Constants of the reorientational response function of carbon disulfide, toluene, and nitrobenzene to Eq. (2). The latter two have been fitted from the references [22–24], whereas the parameters for CS₂ have directly been taken from [20]

Parameter	CARBON DISULFIDE	TOLUENE	NITROBENZENE
A_1 (1/s)	0.4006	0.1265	0.0288
A_2 (1/s)	0.6598	0.3106	0.0930
A_3 (1/s)	1.296	2.646	1.475
t_{diff} (ps)	1.68	5.9	31.8
$t_{rise,1}$ (ps)	0.14	0.15	0.15
t_{int} (ps)	0.40	0.50	0.51
t_{fast} (ps)	0.185	0.10	0.08
$t_{rise,2}$ (ps)	0.15	0.15	0.10

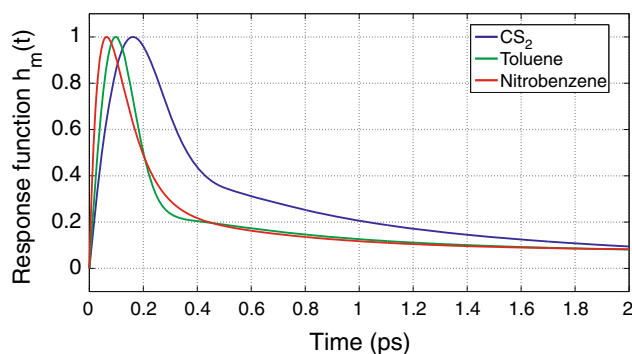


Fig. 3 Reorientational response functions $h_m(t)$ for CS₂, toluene, and nitrobenzene with the constants from Table 1. Nitrobenzene (31.8 ps) has the slowest response time followed by toluene (5.9 ps) and CS₂ (1.68 ps) which becomes more obvious when considering the slope at longer time intervals. For the fastest delayed dynamics, the opposite behavior can be observed

is that the propagation in the capillaries that can also support multi-modal propagation has to be enforced to be single mode in order to distinctively define the mode parameters such as effective mode area and carried power, which are also required to precisely determine the nonlinear refractive index. However, negligible coupling and small power loss from the fundamental mode to the higher-order modes occur due to the small core and large-core-cladding index difference of the investigated liquid-filled capillaries. Hence, if only the fundamental mode is excited at the fiber entrance, the propagation will remain single mode during the entire fiber length. Furthermore, the response function must be known in order to obtain the correct combination of the fractional contribution f_m and the nonlinear refractive index n_{2l} . Another requirement is that the refractive index of the liquid filled into the capillary has to be higher than that of the cladding material fused silica to enable waveguiding by the effect of total internal reflection. In the case of carbon tetrachloride

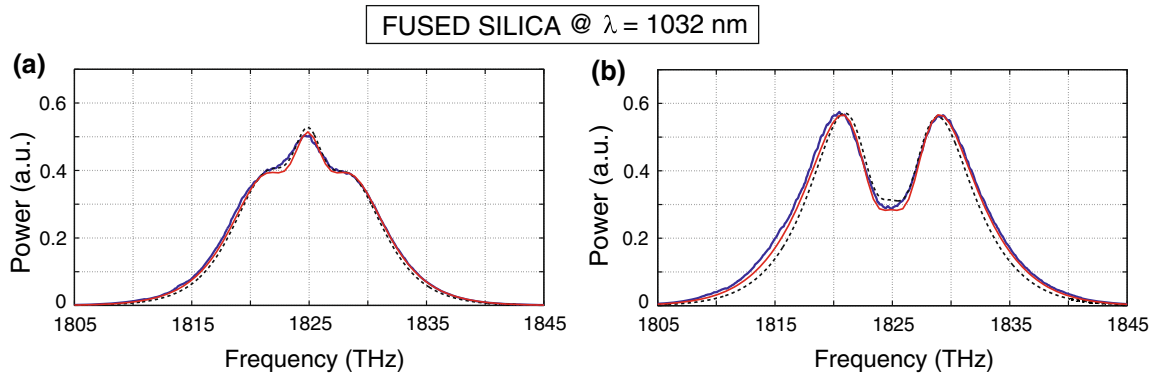


Fig. 4 Comparison between the measured values (*blue curve*), the numerical simulation (*dashed black curve*), and the analytical model [13] (*red curve*) for fused silica. The measurement was conducted with the Yb:KGW oscillator at a wavelength of 1032 nm for an average power of **a** 90 mW and **b** 120 mW. The fiber was 22.5 cm

long. The measured transmitted spectra agree well to both models and prove the application of the analytical model for the evaluation of the nonlinear refractive index of fused silica and confirm the accuracy of the numerical simulations

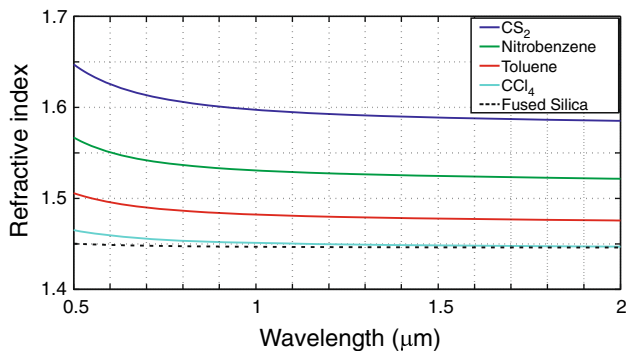


Fig. 5 Linear refractive indices of highly nonlinear liquids [27] in comparison with the cladding material fused silica [28]. All these liquids fulfill the requirement of a higher refractive index with respect to fused silica, whereas CCl₄ is unfeasible for our measurements

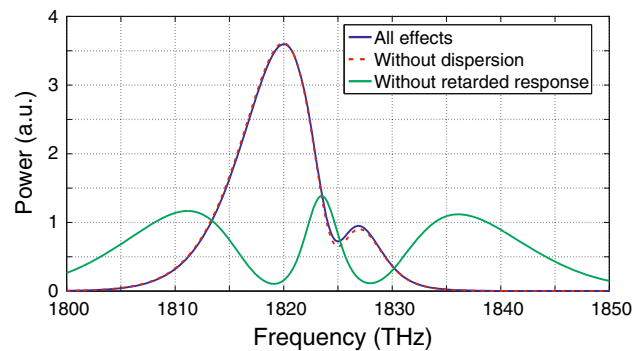


Fig. 6 Comparison between the individual effects of the numerical model for a CS₂-filled capillary fiber with a core diameter of 2 μm at a maximum nonlinear phase shift of $\Phi_{NL,max} = \gamma P_0 L = 3\pi$. Clearly visible is the difference in the spectral shape if the retarded response is considered or not whereas dispersion has only weak influence

(CCl₄), it was not possible to extract n_{2l} due to the weak core-cladding index difference and hence a small value of the V-parameter ($V = 2\pi a/\lambda\sqrt{n_{core}^2 - n_{clad}^2}$ with core radius a) which results in a weak mode confinement. The trend of the linear refractive indices in comparison with fused silica can be seen in Fig. 5.

For our simulations, we implemented the following NLSE to fit our measured spectra [29]:

$$\frac{\partial A}{\partial z} - i \sum_{k=2}^{10} i^k \frac{\beta_k}{k!} \frac{\partial^k A}{\partial T^k} = i\gamma \left(1 + \frac{i}{\omega_0} \frac{\partial}{\partial T} \right) \left(A \int_{-\infty}^{+\infty} R(t') |A(z, T - t')|^2 dt' \right), \tag{3}$$

where $A = A(z, T)$ is the pulse envelope of the electric field, z the propagation distance, and T the time in the co-moving reference frame. β_k is the k^{th} order dispersion

coefficient at center frequency ω_0 , and $\gamma = n_{2l}\omega_0/(cA_{eff})$ denotes the nonlinear parameter with the effective mode area A_{eff} and the vacuum speed of light c . In Eq. (3), absorption is neglected due to the weak absorption coefficients of the liquids and the small fiber lengths used in our experiment [6, 27]. For the calculation of the dispersion coefficients by solving the propagation equation in fibers [25], we use the refractive indices of the liquids from a previous measurement [27] and of fused silica from reference [28] and include the fiber geometry. For all our measurements, we operate in the normal dispersion regime. However, for fiber lengths in the order of several centimeters, dispersion effects do not have much influence on the output spectrum, as can be seen in Fig. 6. The delayed nature of the nonlinear response leads to an energy transfer during propagation to higher wavelengths which is accompanied by a red shift (comparable phenomenon as for the Raman-induced frequency shift). Moreover, the

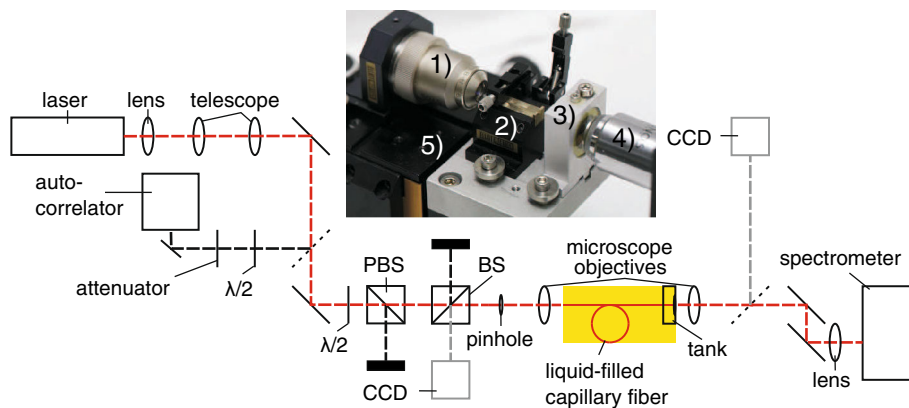


Fig. 7 Experimental setup for nonlinear refractive index measurements. *Inset* Picture of the fiber coupling setup. The laser beam is focused with an aspherical lens (1) free space into the liquid-filled capillary, which is placed on a fiber holder (2). The light from the

fiber end which sticks in the tank (3) is collected with a microscope objective (4). The whole components apart from the outcoupling objective are mounted on a fiber launch stage (5) which allows μm-precise positioning

broadening is diminished in comparison with the neat SPM-induced splitting as observable in Fig. 6.

For the initial pulse form, we use a hyperbolic secant pulse given by

$$A(0, T) = \sqrt{P_0} \operatorname{sech}\left(\frac{T}{T_0}\right), \tag{4}$$

where P_0 denotes the peak power and T_0 the pulse width due to the solitary pump source.

3 Experimental setup

The experimental setup is shown in Fig. 7. A home-built Yb:KGW femtosecond laser oscillator [30] at a wavelength of 1032 nm and a cw-seeded optical parametric amplifier (OPA) at a wavelength of 1560 nm [31] are used as light sources for the determination of the nonlinear refractive index n_{2l} of the liquids.

Because of the sech^2 -shaped laser pulses, the stable intensity, and the pulse durations on the right order of magnitude to observe the impacts of the retarded material response, the laser sources are particularly suitable for the application of nonlinear refractive index measurements. The laser parameters are listed in Table 2.

A lens and a telescope setup are used to provide suitable collimation and beam waist for the 2, 5 and 10 μm core diameters of the capillary fibers used in our experiment. With the position of the rear lens in the telescope setup, the beam diameter can be adapted to the mode field diameter of the particular liquid-filled fiber and the incoupling objective, respectively.

To focus the laser beam to a spot with a size close to the core diameter of the capillary fiber, an aspherical objective is used. Depending on the core diameter, different objective

Table 2 Laser specifications of the two light sources used in our experiment

	Yb:KGW oscillator	OPA
Wavelength λ_0	1032 nm	1560 nm
Average power P_{avg}	7.4 W	150 mW
Pulse duration T_{FWHM}	450 fs	270 fs
Repetition rate f_{rep}	41 MHz	41 MHz

powers are utilized to optimize the focus size as well as the numerical aperture (NA) of the beam to the particular fiber mode. These conditions and a precise beam guidance are essential to only excite the fundamental mode in the multi-mode capable capillary fibers. A further precondition for a high transmission efficiency of the liquid-filled fiber is free space coupling [9], so only one end of the fiber is pushed into a liquid tank.

A necessary quantity for the characterization of the frequency spectrum is the pulse duration which is measured by an autocorrelator and yields $T_{\text{FWHM}} = 450$ fs (at 1,032 nm) and $T_{\text{FWHM}} = 270$ fs (at 1,560 nm), respectively (see Fig. 8).

With a half-wave plate in combination with a polarizing beam splitter (PBS), the power launched into the fiber can be adjusted. A second beam splitter (BS) provides the ability to control the free space coupling of the laser beam into the liquid-filled capillary. The reflected laser spot from the fiber surface as well as the light from a lamp, illuminating the fiber from the backside, is recorded by a CCD camera. This procedure helps to preset the spatial position of the focus spot with respect to the fiber end face and eventually to cope with the challenge of coupling into a 2 μm fiber core. For the OPA pumping wavelength at 1560 nm, where the CCD camera is insensitive, the fiber

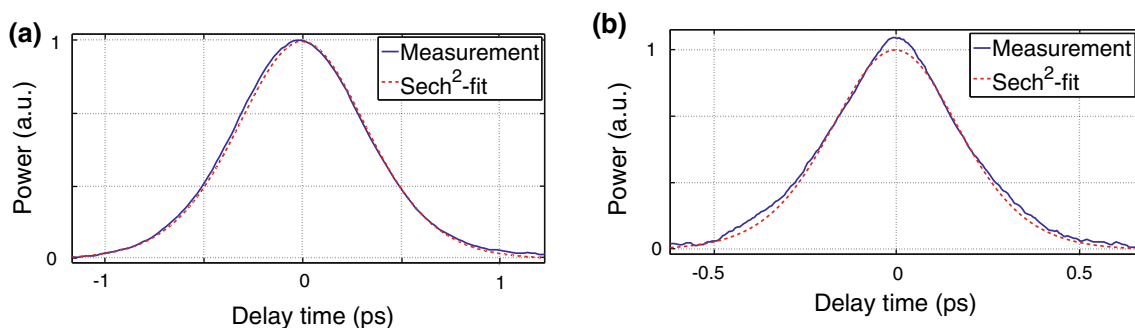


Fig. 8 Autocorrelation measurements of the **a** Yb:KGW laser and **b** OPA. The pulse durations are extracted from a sech^2 fit. The latter pulse is nearly sech^2 -shaped and slightly chirped

position was preset by the collinearly overlapped beam from the Yb:KGW oscillator.

Due to the strong divergence of the fiber output beam, the fiber end has to be placed closely to the glass plate window of the liquid tank. The liquid is sucked into the fiber by capillary force. A 40x outcoupling microscope objective is mounted close to the tank. With a flip mirror, an image of the mode profile at the fiber end can be obtained by a CCD camera to control the modal distribution.

The average power is measured behind the outcoupling objective and finally directly behind the fiber tank to determine the outcoupling losses of the objective. To derive the power at the fiber entrance, the reflection losses of about 3.5 % at the glass plate window of the fiber tank have to be taken into account.

Finally, the laser beam is focused directly into an optical spectrum analyzer. Depending on the recorded wavelength range, the Ando AQ-6315E spectrometer with a measuring range from 350 up to 1750 nm or the Yokogawa AQ6375 spectrometer with a measuring range from 1,200 up to 2,400 nm is employed.

The overall transmission through the liquid-filled capillary fiber, measured before the incoupling and behind the outcoupling objective, is about 40–50 % for a 2 μm core and 55–65 % for a 10 μm core. No notable change in transmission is observed for increased power values indicating that nonlinear absorption does not play a role in our investigated power regime. The coupling efficiency is mainly determined by the curvature of the liquid at the free space fiber incoupling end and a clean cleave. The losses due to the glass plate and the outcoupling microscope objective are about 20–35 % with respect to the measured output power behind the objective depending on the wavelength, core diameter, and liquid.

The following parameters have to be determined and are inserted into the MATLAB code:

- Pulse shape (sech)
- Fiber length (L)
- Core diameter ($2a$)
- Core medium (n_{liq})
- Pulse width (T_0)
- Central wavelength (λ_0)
- Average power (P_{avg})
- Repetition rate (f_{rep})
- Effective mode area (A_{eff})

The pulse shapes of the Yb:KGW oscillator and also the OPA are hyperbolic secant as determined by an autocorrelation measurement, whereas the latter pulse is slightly chirped as can be seen in Fig. 8b). So we determine the Fourier transformed pulse duration of the OPA signal from the experimental spectrum (180 fs) to obtain the correct spectral width of the input spectrum in the simulation. However, to maintain the temporal pulse width measured via the autocorrelator, we have to apply an additional chirp of $C = 10,000 \text{ fs}^2$ in the simulation code. With this procedure, we obtain very good agreement for the spectral as well as for the temporal pulse shape of the incident beam. The fiber length is kept small to obtain only weak dispersion effects but long enough to record a clear frequency splitting with the available laser pump power. The actual core diameters of the commercially available capillaries are given by the manufacturer Polymicro Technologies [32] and listed in Table 3. They deviate from their specified inner diameter within $\pm 0.5 \mu\text{m}$. We choose the capillaries with specified core diameters of 2, 5 and 10 μm , depending on the liquid and pump wavelength to achieve a good mode confinement in the liquid core. The core medium linear refractive indices have been measured in previous work [27]. The pulse width is controlled before every measurement series. The central wavelength can be determined by the spectrometer at very low intensities. The average power inserted into the simulation is deduced from the measured output power, corrected for the losses due to

Table 3 Effective mode field areas in μm^2 of the fundamental mode for CS_2 , nitrobenzene, and toluene for the different actual core diameters of the capillaries calculated at the Yb:KGW laser wavelength of 1,032 nm and the OPA wavelength of 1,560 nm, respectively, by the software Fimmwave [33]

Identification	CARBON DISULFIDE	NITROBENZENE	TOLUENE
1.5 μm -fiber	– / 4.23	– / 6.58	– / 47.57
1.8 μm -fiber	2.17 / 4.42	2.77 / 6.19	5.48 / 21.37
4.5 μm -fiber	8.97 / 11.12	9.77 / 12.66	11.87 / 16.82
9.5 μm -fiber	37.3 / 32.34	38.8 / 34.53	42.10 / 39.63

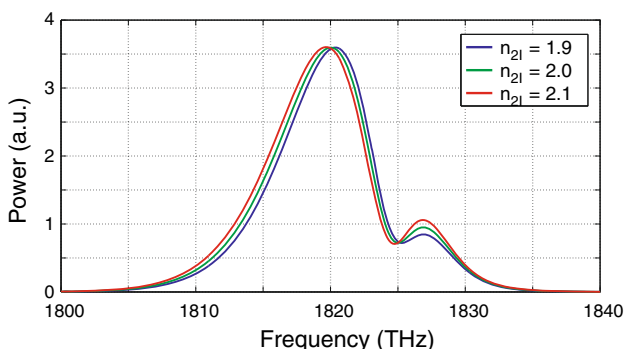


Fig. 9 Effect of the nonlinear refractive index n_{21} on the numerical model for a CS_2 -filled capillary fiber with a core diameter of 2 μm at a maximum nonlinear phase shift of about $\Phi_{\text{NL,max}} = 3\pi$. The fraction of the retarded response and the other parameters remain constant. The spectra are normalized to the green curve and the corresponding nonlinear refractive indices are given in units of $10^{-18} \text{m}^2/\text{W}$

the outcoupling objective and the glass plate. The repetition rate is obtained by an oscilloscope. The effective mode area is calculated via the software Fimmwave [33]. Due to the fact that the refractive index profile of the liquid-filled capillary is similar to a step-index fiber, the software calculates the actual mode field profile from the stated core diameter and refractive indices of the core liquid and the cladding material fused silica. The effective mode areas for the numerical simulation are listed in Table 3.

The following two parameters are adjusted in such a way that an ideal agreement between the measured and simulated spectral form is achieved:

- Nonlinear refractive index (n_{21}),
- Fraction of the retarded response (f_m).

The influence of these two parameters on the spectrum for a fixed given configuration can be seen in Fig. 9 for n_{21} and in Fig. 10 for f_m .

With the nonlinear refractive index, one can regulate the curvature of the second weaker peak and the width of the whole spectrum, whereas the coefficient for the reorientational function controls the relative height to the higher

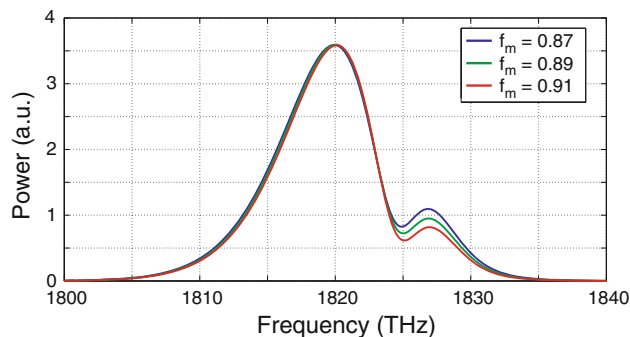


Fig. 10 Effect of the nonlinear retarded response fraction f_m on the numerical model for a CS_2 -filled capillary fiber with a core diameter of 2 μm at a maximum nonlinear phase shift of $\Phi_{\text{NL,max}} = 3\pi$. The nonlinear refractive index and the other parameters remain constant. The spectra are normalized to the green curve

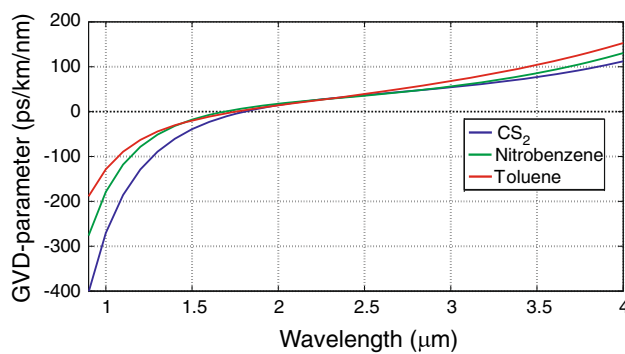


Fig. 11 GVD for liquid-filled capillary fibers with a core diameter of 5 μm . The zero dispersion boundary is marked with the black-dotted line. The ZDWs are as follows: CS_2 , 1.80 μm ; nitrobenzene, 1.69 μm ; and toluene, 1.76 μm . For the capillaries with a core diameter of 2 and 10 μm the ZDWs are higher. Thus, we operate at both pump wavelengths in the normal dispersion regime

frequency peak. Thus, with these two adapted parameters, the simulated spectrum can be fitted to the measured one.

The group velocity dispersion (GVD) parameter (given by $D = -\frac{2\pi c}{\lambda^2} \frac{d^2\beta}{d\omega^2}$) is negative for all liquids at each core diameter at both measured wavelengths. The lowest zero dispersion wavelength (ZDW) appears at a core diameter of 5 μm but not below a wavelength of around 1.7 μm . This means that we are in the normal dispersion region and can expect a strong red shift. The dispersion behavior of the fundamental mode for a 5 μm capillary is shown in Fig. 11.

At a wavelength of 1,032 nm, only the 2 μm toluene-filled capillary fulfills the requirement of $V < 2.405$ which assures operation under single-mode conditions. At 1,560 nm, all liquid-filled capillaries with a core diameter of 2 μm fulfill the single-mode condition, whereas the V-parameter of toluene is so small that the mode energy is no longer propagating almost completely in the liquid core (see Fig. 12). For the two longer core diameters, the

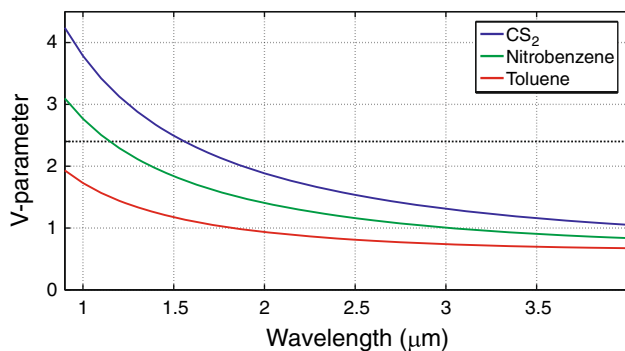


Fig. 12 V-parameter for core liquid-filled capillary fibers with a core diameter of 2 μm . The single-mode boundary at $V = 2.405$ is marked with the black-dotted line. At the pump wavelength of 1,032 nm, only the toluene-filled capillary is single mode, whereas at the higher OPA wavelength of 1,560 nm, all liquids are below the single-mode boundary. However, for toluene, the V-parameter is in the latter case close to 1 which results in a very weak energy confinement in the liquid core. For the two longer core diameters, we have at both laser wavelengths a V-parameter that allows multi-mode propagation

V-parameter allows multi-mode propagation at both laser wavelengths. However, through careful coupling, we are able to only excite the fundamental mode.

4 Experimental data and numerical nonlinear refractive index results

To obtain a noticeable frequency splitting, it turns out that the maximum nonlinear phase shift has to be in the order of $\Phi_{\text{NL,max}} = \gamma P_0 L = 3\pi$. The clearest broadening is obtained by using fiber capillary lengths on the order of several centimeters. At both wavelengths, several measurements of the output spectrum at different power levels, core diameters, and fiber lengths are taken. Each recorded spectrum is then carefully analyzed by inserting the measured parameters in a MATLAB code and fitting the simulated spectrum to the measured one by adapting n_{21} and f_m , respectively. Finally, for each liquid, an arithmetic average of the nonlinear refractive index n_{21} and the fractional contribution f_m is calculated. By far more spectra are evaluated than actually displayed in Figs. 13–18. We conduct at least 5, in some cases, up to 24 measurements for each liquid at each investigated wavelength.

To obtain an estimate of the uncertainty of the nonlinear refractive index of the liquids, we have to consider the error of the nonlinear phase shift which is governed by the quality of the measured broadened spectra. Furthermore, the precision of the other parameters, which are necessary to calculate the nonlinear refractive index from the nonlinear phase shift extracted from the fits have to be taken into account.

When the nonlinear phase shift is determined by the fit, the following formula to deduce the error of the nonlinear refractive index can be used

$$n_{21} = \frac{\Phi_{\text{NL,max}} \lambda A_{\text{eff}} T_{\text{FWHM}} f_{\text{rep}}}{1.76\pi P_{\text{avg}} L}. \quad (5)$$

The uncertainty can now be determined by error propagation. Actually we have to vary each parameter inserted in the simulation within the error bars because of the interplay between dispersive and several nonlinear effects and then performing several fits of the experimental curves to estimate the error on the nonlinear refractive index. However, by testing the simulation, we see that changes for the inserted parameters directly influence the nonlinear refractive index and hence error propagation of Eq. (5) delivers a good estimation of the uncertainties of n_{21} .

The precision of the actual fitting parameter $\Phi_{\text{NL,max}}$ is given by the possible deviations of the perfect single-mode operation and the fraction of the retarded material response. However, by performing several fits, the error of the nonlinear refractive index related to the uncertainty of the recorded spectrum and hence the nonlinear phase shift can be contained and good estimated by the standard error of the average value. The uncertainty is on the order of 2 – 10% depending on the quality of the measurement series.

The other separately measured quantities, which are also crucial to determine the uncertainty of n_{21} with Eq. (5) are the effective mode area A_{eff} , the average power P_{avg} , the pulse duration T_{FWHM} , and the fiber length L . Additional uncertainties connected with the central laser wavelength λ , and the repetition rate f_{rep} are negligibly small.

The deviations in the effective mode area, which one calculates from the given core radius and the refractive indices of the core and the cladding, are about 5%. They can arise from temperature variations, which affect the refractive index, and from deviations in the actual core diameter. The average power is measured by a thermal power meter, and the deduced average power at the fiber entrance is corrected for the outcoupling losses. The total error referred to the power determination is considered to be about 8% including the uncertainties of the absolute power value of the device and of the measured outcoupling losses. The pulse duration is determined by an autocorrelator with typical errors of around 2%. The uncertainty concerning the determination of the fiber length is about 0.5 mm, which corresponds to 1 – 2% for our used fiber lengths.

The precision of the fractional contribution of the retarded response f_m is determined by the standard deviation of the average value.

In the following typical transmitted spectra for each liquid at both laser wavelengths are shown demonstrating a

clear asymmetrical broadening attributed to the retarded response effect.

The spectral broadening in the liquid-filled capillary fibers due to the effect of self-phase modulation is accompanied by the effect of the slow nonlinear material response. Therefore, the behavior of the spectral evolution during the pulse propagation in the fiber is quite different compared to symmetrical broadening attributed to neat self-phase modulation in glass fibers or liquid acetone [13, 34–36]. Rather, primarily a second weaker peak is observable at the short wavelength side, whereas the main peak shifts always further red when increasing the pump power. This arises from the fact that energy is transferred to the liquid molecules during the excitation of reorientational motions. This is also the reason why the transmitted spectrum is asymmetric, whereas the multi-peak SPM structure appears in a weaker distinctive manner again. However, due to the extremely large nonlinear refractive indices of the investigated liquids, only low average powers, e.g., in the range of 1 mW for the 2 μm CS₂-filled core, are necessary (corresponding to a peak power of 50 W) to realize an adequate frequency broadening. This means that the second peak must begin to appear for adjusting the relative height of the main peak with reference to the second weaker peak by means of the fractional

contribution. Subsequently, the nonlinear refractive index has to be adapted properly. Only such output spectra have been evaluated, in which no more than two spectral peaks are visible to reduce the influence of higher power effects and interplay between dispersion and nonlinear effects. Also the fitting procedure at still higher power levels turns out to be more difficult (adopting three or more peak heights) which would cause less precise fitting results. Hence, we limit the evaluation to the above-mentioned power regime where an adequate spectral splitting enable us to obtain accurate fitting results. Additionally, relatively small fiber lengths of around 3–4 cm are studied to be in the regime where dispersion effects play a minor role. For longer fibers in the range of 10 cm, especially for the 10 μm core diameter, problems to attain a clear single-mode spectrum appear.

In general, the attained overall agreement between experiment and simulation is excellent for all our investigated liquids at both laser wavelengths.

4.1 Carbon disulfide

Figure 13 shows the experimental transmitted spectra (blue curves) at a pump wavelength of 1,032 nm for different average powers which are evaluated with the numerical

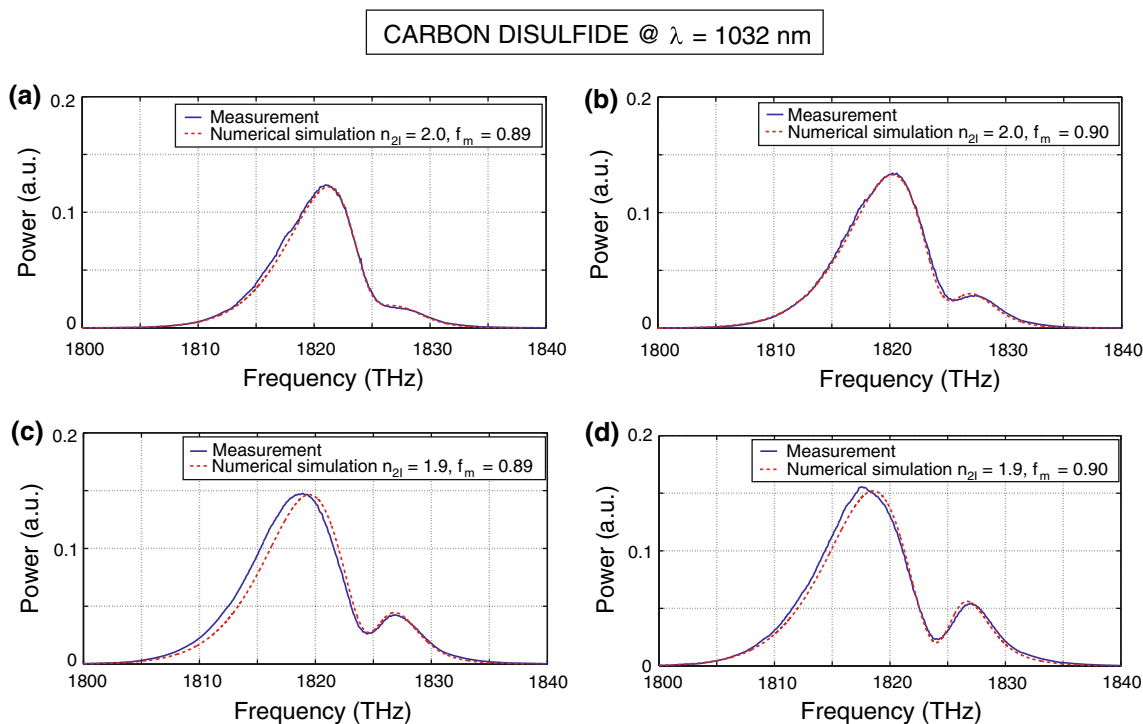


Fig. 13 Fitting results with the numerical simulation (red dashed curves) at a wavelength of 1,032 nm for a 2 μm CS₂-filled capillary fiber for different average power levels of **a** 0.50 mW, **b** 0.60 mW, **c** 0.70 mW, **d** 0.80 mW. The corresponding nonlinear refractive indices are given in units of 10⁻¹⁸ m²/W. The measured values of the

3.9-cm-long fiber are illustrated in blue. The pulse duration of the Yb:KGW oscillator was $T_{FWHM} = 450$ fs. The achieved agreements are excellent and also the reorientational fraction as well as the nonlinear refractive indices lie in a close range for all four displayed power levels

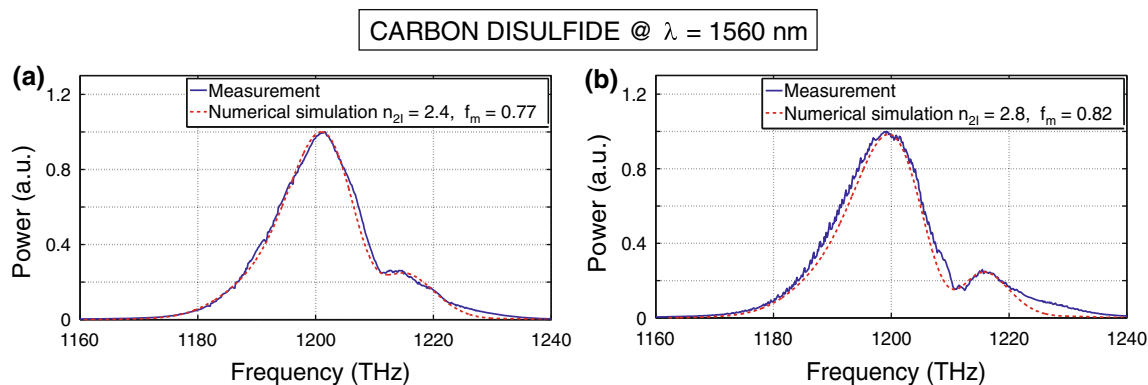


Fig. 14 Fitting results with the numerical simulation (*red dashed curves*) at a wavelength of 1,560 nm for a 5 μm CS_2 -filled capillary fiber for different average power levels of **a** 7.0 mW, **b** 8.0 mW. The corresponding nonlinear refractive indices are given in units of $10^{-18} \text{ m}^2/\text{W}$. The measured values of the 1.95- and 1.9-cm-long fiber,

model (*red dashed curves*) that solves the generalized NLSE [(Eq. (3))] with a split-step Fourier method as described in the previous section. Fitting parameters are the nonlinear refractive index n_{2I} , as well as the fraction of the reorientational contribution f_m , which are given in the legend. The measurements are conducted for a 3.9-cm-long CS_2 -filled capillary with a core diameter of 2 μm .

The quality of the agreement between the measurements and the simulations is excellent. The fraction of the reorientational response is adjusted for each measurement and lies well within the predicted range of about 0.89 [6] with variations of only 1%. The agreement remains quite good also at the two highest average powers of 0.70 and 0.80 mW (c),(d), whereas the nonlinear refractive index drops from $2.0 \times 10^{-18} \text{ m}^2/\text{W}$ to $1.9 \times 10^{-18} \text{ m}^2/\text{W}$. At a core diameter of 10 μm , the deduced fractional contributions are somewhat lower and altogether an averaged nonlinear refractive index for CS_2 at a wavelength of 1,032 nm is obtained with a precision on the order of $(2.2 \pm 0.4) \times 10^{-18} \text{ m}^2/\text{W}$ with an averaged fractional reorientational contribution of 0.88.

From the measurement at the OPA wavelength of 1560 nm somewhat higher, nonlinear refractive index values are deduced as can be seen in Fig. 14 for a 5 μm CS_2 -filled capillary. Also the fractional contribution of the retarded response has changed to lower values. The agreement between experiment and simulation remains very good, whereas at the wing of the long frequency side additional components appear. They can arise from deviations of the incident pulse from the perfect sech^2 -shape. From several measurements, we determine an average nonlinear refractive index of $(2.7 \pm 0.5) \times 10^{-18} \text{ m}^2/\text{W}$ and an average reorientational contribution of 0.81.

The values for n_{2I} of carbon disulfide found in the literature are relatively widespread. In the paper of

Sheik-Bahae [37], nonlinear refractive index values of $3.4 \times 10^{-18} \text{ m}^2/\text{W}$ measured at 1060 nm and of $3.9 \times 10^{-18} \text{ m}^2/\text{W}$ at a wavelength of 10.6 μm were reported. However, longer pulse durations of several ps were used. An even higher value of n_{2I} is listed in [1] of $5.2 \times 10^{-18} \text{ m}^2/\text{W}$ also at a higher pulse duration on the order of 10 ps at a laser wavelength of 1064 nm. However, at comparable pulse durations of 400 and 500 fs at a wavelength of around 500 nm nonlinear refractive index data of $4.1 \times 10^{-18} \text{ m}^2/\text{W}$ and $1.3 \times 10^{-18} \text{ m}^2/\text{W}$ are given in [14].

For even shorter pulse durations of around 100 fs in the visible wavelength region, the value of n_{2I} ranges between $0.25 \times 10^{-18} \text{ m}^2/\text{W}$ and $1.2 \times 10^{-18} \text{ m}^2/\text{W}$ [14].

This makes it evident that for shorter pulse durations, the nonlinear refractive index decreases due to the weaker contribution of the reorientational response as also observed in [38]. We also can observe a reduction of the reorientational fraction of 7% for shorter pulses but at a n_{2I} value increased by about 20%, which can arise from its wavelength dependence.

Altogether, it is comprehensible that our measured values of n_{2I} are lower compared to the former measurements in the ps-range, but no experiment has been carried out at comparable parameters as in our case.

4.2 Nitrobenzene

The recorded spectra for the liquid with the slowest nonlinear response, nitrobenzene, are displayed in Fig. 15. The measurement is conducted at a wavelength of 1032 nm with capillaries of 10 μm core diameter. The reorientational fraction is the highest among the three investigated liquids with an average value of 0.97. Also the nonlinear refractive index is quite high but varies for the different measurements as can be seen between Fig. 15 a–d. We calculate an

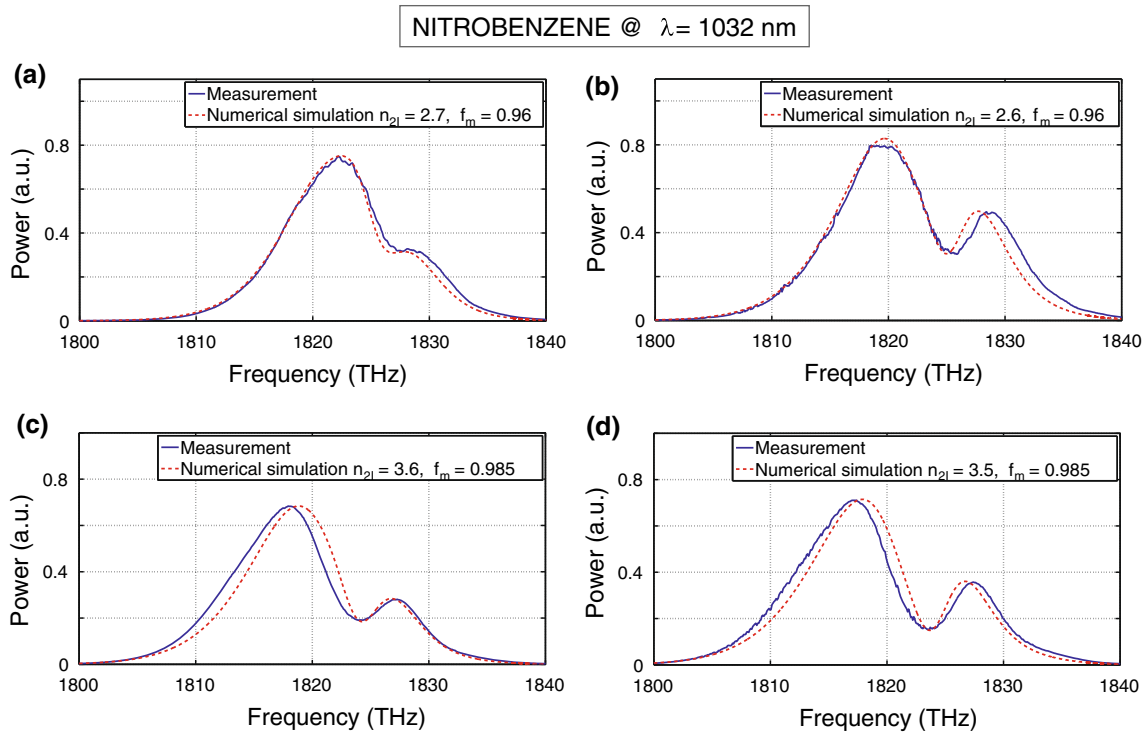


Fig. 15 Fitting results with the numerical model (red dashed curves) at 1,032 nm for a 10 μ m nitrobenzene-filled capillary fiber for different average power levels of **a** 35 mW, **b** 45 mW, **c** 35 mW, and **d** 40 mW. For the first two measurements, the fiber length is 3.7 cm, whereas for the last two, the fiber is 3.6 cm long. The pulse duration of the Yb:KGW oscillator is equal to $T_{\text{FWHM}} = 430$ fs, and

$T_{\text{FWHM}} = 450$ fs, respectively. The corresponding nonlinear refractive indices are given in units of $10^{-18} \text{ m}^2/\text{W}$. The quality of the agreement between the measurement values (blue curves) and the simulation is fine; however, the nonlinear refractive index values obtained from the simulation differ by 30 %, whereas the fractional contribution varies only by about 3 %

averaged nonlinear refractive index with a higher uncertainty of $(3.2 \pm 0.8) \times 10^{-18} \text{ m}^2/\text{W}$.

For the measurements at a wavelength of 1560 nm, the nonlinear refractive index drops by around 40 % to an average value of $(2.0 \pm 0.5) \times 10^{-18} \text{ m}^2/\text{W}$, as can be seen in Fig. 16. As in the former case, the n_{21} values differ a lot which leads to an overall uncertainty of 27 %. Also the second weaker peak in the spectrum is quite high in contrast to the measurement at a wavelength of 1032 nm which may be caused by higher-order modes. However, the average reorientational contribution is still 0.86.

In contrast to carbon disulfide the nonlinear refractive index of nitrobenzene declines at the higher wavelength. This may arise from the stronger pulse duration dependence, which hinders the liquid molecules to reorient themselves for shorter pulse durations. The nonlinear refractive index values quoted in the literature lie between $2.4 \times 10^{-18} \text{ m}^2/\text{W}$ [15] and $6.9 \times 10^{-18} \text{ m}^2/\text{W}$ [1] measured with pulse durations of several picoseconds.

4.3 Toluene

The same spectral broadening behavior as for the two previous liquids is observed for toluene but with higher

required input powers. In Fig. 17, the transmitted spectra (blue curves) for a capillary with a core diameter of 2 μ m at a wavelength of 1,032 nm are shown for different output average powers and fiber lengths.

The comparison with the numerical value demonstrates good conformity. The fraction of the reorientational contribution is in the same range as for carbon disulfide on the order of 90 %. However, much lower values for the nonlinear refractive index are obtained. In the measurement results for the 2 μ m capillary fiber relatively widespread, nonlinear refractive index data in the range between 0.51×10^{-18} and $0.67 \times 10^{-18} \text{ m}^2/\text{W}$ are obtained despite the fact that in the 2 μ m toluene-filled fiber only the fundamental mode can propagate.

For the measurements with the 10 μ m core diameter, nonlinear refractive indices in the range between 0.58×10^{-18} and $0.65 \times 10^{-18} \text{ m}^2/\text{W}$ are extracted at somewhat lower reorientational fractions. The simulated spectra match the measured ones quite well.

An average nonlinear refractive index for toluene of $0.62 \times 10^{-18} \text{ m}^2/\text{W}$ is obtained at a wavelength of 1032 nm from several measurements at both fiber diameters. The corresponding averaged fractional contribution is 0.88.

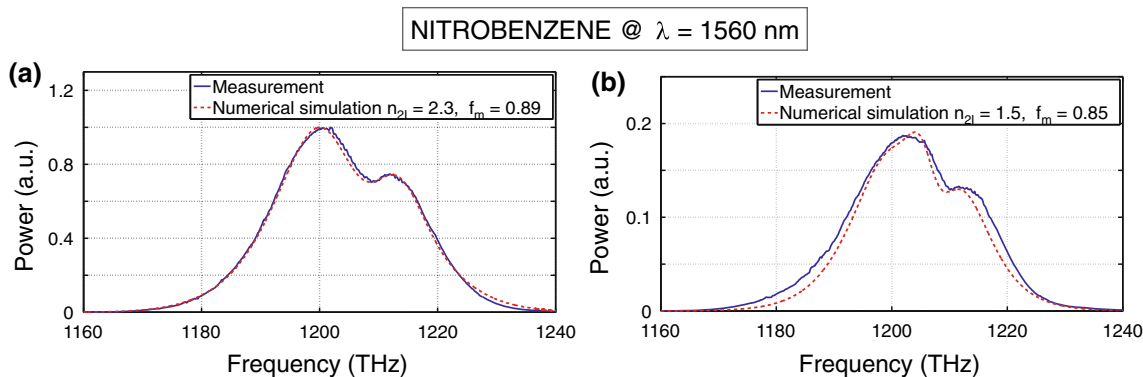


Fig. 16 Fitting results with the numerical simulation (red dashed curves) at a wavelength of 1,560 nm for nitrobenzene-filled capillary fibers with a core diameter of 2 and 5 μm for different average power levels of **a** 5.0 mW, **b** 12.5 mW. The corresponding nonlinear refractive indices are given in units of $10^{-18} \text{ m}^2/\text{W}$. The measured

values of the 4.2 and 2.5-cm-long fiber, respectively, are illustrated in blue. The pulse duration of the OPA is for both measurements $T_{\text{FWHM}} = 265$ fs. The achieved agreements are quite good, whereas the fractional contribution is about 10 % weaker as for the $T_{\text{FWHM}} = 430$ fs pulses at a wavelength of 1,032 nm

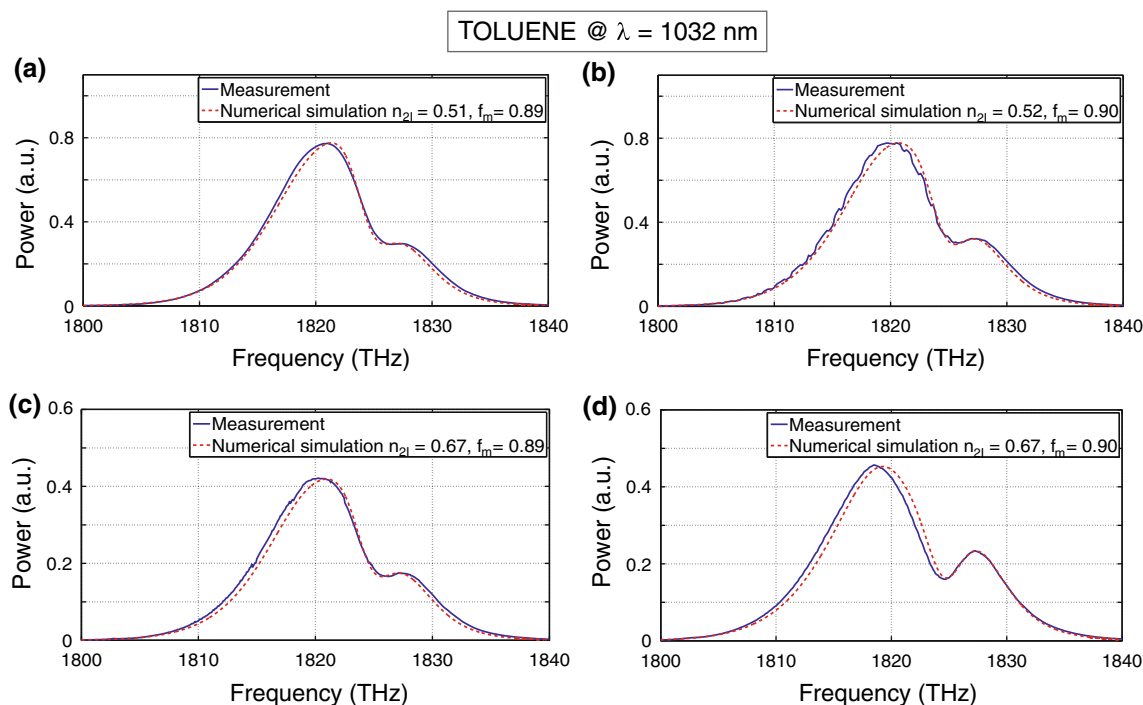


Fig. 17 Fitting results with the numerical model (red dashed curves) at 1032 nm for a 2 μm toluene-filled capillary fiber for different average power levels of **a** 8.0 mW, **b** 8.5 mW, **c** 6.0 mW, and **d** 7 mW. For the first two measurements, the fiber length is 3.7 cm, whereas for the last two the fiber is 3.9 cm long. The pulse duration of the Yb:KGW oscillator is for both measurement series (blue curves)

equal to $T_{\text{FWHM}} = 430$ fs. The corresponding nonlinear refractive indices are given in units of $10^{-18} \text{ m}^2/\text{W}$. The conformity with the simulation is quite good; however, the nonlinear refractive index values obtained from the simulation differ by 30 % in spite of the fact that only the fundamental mode can propagate

The precision is on the order of $(0.62 \pm 0.12) \times 10^{-18} \text{ m}^2/\text{W}$ and comparable to the uncertainty of carbon disulfide.

Figure 18 shows the results for the measurement at a wavelength of 1560 nm. The deduced average nonlinear

refractive index is nearly the same as for the lower wavelength with a value of $(0.59 \pm 0.12) \times 10^{-18} \text{ m}^2/\text{W}$. However, the retarded fractional contribution has a reduced value of only 0.70, which is a decrease of 0.18. The fits agree very well with the experimental curves.

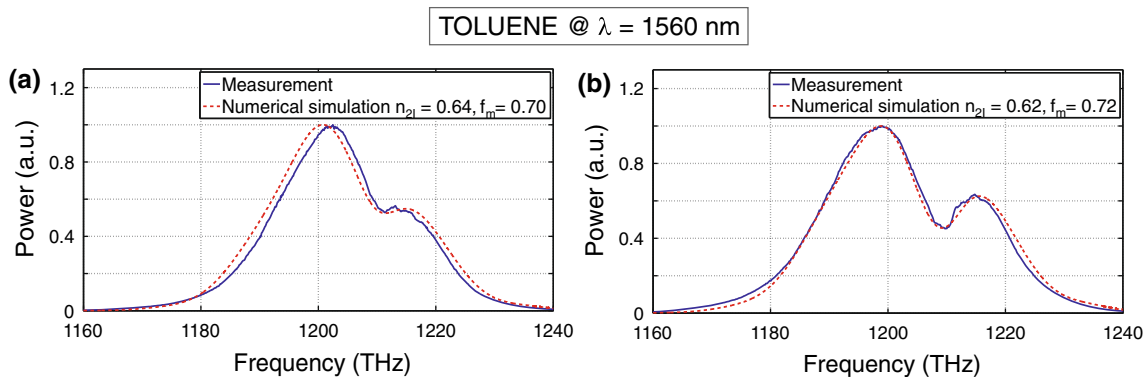


Fig. 18 Fitting results with the numerical simulation (red dashed curves) at a wavelength of 1,560 nm for a 5 μm toluene-filled capillary fiber for different average power levels of **a** 20 mW, **b** 24 mW. The corresponding nonlinear refractive indices are given in units of $10^{-18} \text{ m}^2/\text{W}$. The

measured values of the 3.1-cm-long fiber are illustrated in blue. The pulse duration of the OPA is $T_{\text{FWHM}} = 270$ fs. The achieved agreements are quite good, whereas the fractional contribution is much weaker as for the $T_{\text{FWHM}} = 430$ fs pulses at a wavelength of 1,032 nm

Table 4 Results for the nonlinear refractive indices and fractional contributions at the two pump wavelengths of 1032 nm and 1560 nm measured with 450 fs and 270 fs pulse durations, respectively. The corresponding n_{21} values are given in units of $10^{-18} \text{ m}^2/\text{W}$. The uncertainty for the nonlinear refractive index values varies between 18 and 27 % depending on the quality of the measurement series

	n_{21} @ 1032 nm	f_m @ 1032 nm	n_{21} @ 1560 nm	f_m @ 1560 nm
CS ₂	2.2 ± 0.4	0.88 ± 0.01	2.7 ± 0.5	0.81 ± 0.01
Nitrobenzene	3.2 ± 0.8	0.97 ± 0.01	2.0 ± 0.5	0.86 ± 0.02
Toluene	0.62 ± 0.12	0.88 ± 0.01	0.59 ± 0.12	0.70 ± 0.01

For toluene, the same behavior of the literature values is observable as for the other two liquids. For ps pulses, the nonlinear refractive index is higher on the order of $1.7 \times 10^{-18} \text{ m}^2/\text{W}$ [1]. For a comparable pulse duration of 500 fs, a value of $0.27 \times 10^{-18} \text{ m}^2/\text{W}$ is reported in [14] at a laser wavelength of about 500 nm. For even shorter pulses, the given nonlinear refractive index values drop to 0.09×10^{-18} and $0.13 \times 10^{-18} \text{ m}^2/\text{W}$ [14] at a wavelength of 800 nm.

Thus, our value lies clearly below the ps measurement value, but above the reported value at comparable pulse duration. Moreover, we could confirm the tendency of an around 4–times lower nonlinear refractive index of toluene compared to CS₂ for the same experimental conditions.

5 Conclusion

In summary, in this paper, an experimental setup to determine the nonlinear refractive index and the contribution of the retarded response of carbon disulfide, nitrobenzene, and toluene is presented. Evaluating the measured spectrum, transmitted through the liquid-filled capillaries, with a fitted spectrum based on numerical simulation

provides a powerful tool to determine the nonlinear properties of the liquids with good precision.

The obtained results from the measurements at both pump laser sources at a wavelength of 1032 nm and 1560 nm are summarized in Table 4.

In general, for all three liquids, the fraction of the retarded response decreases for the OPA measurement in contrast to the measurement with the Yb:KGW laser oscillator which can be explained by the shorter pulse duration. However, this does not lead to a decline of the nonlinear refractive index for all liquids. Instead, for CS₂ a 25 % higher n_{21} value could be deduced. This may arise from the wavelength dependence in accordance with the observation in Ref. [37] for CS₂ at wavelengths of 532, 1,064 nm, and 10.6 μm. Overall, lower nonlinear refractive indices are obtained than those reported in the literature measured with sub-nanosecond pulses. Averaging over several measurements at different power levels, core diameters, and fiber lengths, values with high precision can be obtained.

The enhanced nonlinear optical properties by the retarded reorientational response of the liquid molecules remain quite high also for femtosecond pulses in the near-infrared spectral regime. Knowing the nonlinear properties of liquid-filled capillary fibers opens the way to generate

ultrabroadband light sources for the near- and mid-infrared spectral region.

Acknowledgments The authors would like to thank M. Abdou Ahmed from the IFSW for valuable advice and calculating the mode field areas. This work has been supported financially by DFG, BMBF, GIF, ERC, BW-Stiftung, and Alexander von Humboldt Stiftung.

References

- P.P. Ho, R.R. Alfano, *Phys. Rev. A* **20**, 2170 (1979)
- D. Lin-Vien, N.W. Colthup, W.G. Fateley, J.G. Grasselli, *The handbook of infrared and Raman frequencies of organic molecules* (Wiley, Hoboken, 1991)
- O.P. Kulkarni, V. Alexander, M. Kumar, M.J. Freeman, M.N. Islam, F.L. Terry Jr, M. Neelakandan, A. Chan, *J. Opt. Soc. Am. B* **28**, 2486 (2011)
- Y. Yu, X. Gai, T. Wang, P. Ma, R. Wang, Z. Yang, D.-Y. Choi, S. Madden, B. Luther-Davies, *Opt. Mat. Express* **3**, 1075 (2013)
- M. Vieweg, T. Gissibl, S. Pricking, B.T. Kuhlmeier, D.C. Wu, B.J. Eggleton, H. Giessen, *Opt. Express* **18**, 25232 (2010)
- R. Zhang, J. Teipel, H. Giessen, *Opt. Express* **14**, 6800 (2006)
- J. Bethge, A. Husakou, F. Mitschke, F. Noack, U. Griebner, G. Steinmeyer, J. Herrmann, *Opt. Express* **18**, 6230 (2010)
- D. Churin, T.N. Nguyen, K. Kieu, N. Peyghambarian, *Opt. Mat. Express* **3**, 1358 (2013)
- K. Kieu, L. Schneebeli, R.A. Norwood, N. Peyghambarian, *Opt. Express* **20**, 8148 (2012)
- L. Xiao, N.V. Wheeler, N. Healy, A.C. Peacock, *Opt. Express* **21**, 28751 (2013)
- M. Vieweg, S. Pricking, T. Gissibl, Y.V. Kartashov, L. Torner, H. Giessen, *Opt. Lett.* **37**, 1058 (2012)
- C.J. Pouchert, *The aldrich library of infrared spectra* (Aldrich Chemical Co., Milwaukee, 1981)
- M.C.P. Huy, A. Baron, S. Lebrun, R. Frey, P. Delaye, *J. Opt. Soc. Am. B* **27**, 1886 (2010)
- S. Couris, M. Renard, O. Faucher, B. Lavorel, R. Chaux, E. Koudoumas, X. Michaut, *Chem. Phys. Lett.* **369**, 318 (2003)
- M.J. Weber, *Handbook of optical materials* (CRC Press, Boca Roton, 2003)
- S. Pekarek, A. Klenner, T. Stüdmeyer, C. Fiebig, K. Paschke, G. Erbert, U. Keller, *Opt. Express* **20**, 4248 (2012)
- D. McMorrow, W.T. Lotshaw, G.A. Kenney-Wallace, *J. Quantum Electron.* **24**, 443 (1988)
- R.W. Boyd, *Nonlinear Optics*, (Academic Press, 2008), Chap. 4.4
- R.V.J. Raja, A. Husakou, J. Hermann, K. Porsezian, *J. Opt. Soc. Am. B* **27**, 1763 (2010)
- I.A. Heisler, R.R.B. Correia, T. Buckup, S.L.S. Cunha, *J. Chem. Phys.* **123**, 054509 (2005)
- R.H. Stolen, J.P. Gordon, W.J. Tomlinson, H.A. Haus, *J. Opt. Soc. Am. B* **6**, 1159 (1989)
- P. Wiewior, C. Radzewicz, *Optica Applicata* **30**, 103 (2000)
- Y.J. Chang, E.W. Castner, *J. Phys. Chem.* **100**, 3330 (1996)
- W.T. Lotshaw, D. McMorrow, C. Kalpouzos, G.A. Kenney-Wallace, *Chem. Phys. Lett.* **136**, 323 (1987)
- G.P. Agrawal, *Nonlinear fiber optics* (Academic Press, Newyork, 2007)
- J.M. Dudley, G. Genty, S. Coen, *Rev. Mod. Phys.* **78**, 1135 (2006)
- S. Kedenburg, M. Vieweg, T. Gissibl, H. Giessen, *Opt. Mat. Express* **2**, 1588 (2012)
- I.H. Malitson, *J. Opt. Soc. Am.* **55**, 1205 (1965)
- S. Pricking, H. Giessen, *Opt. Express* **19**, 2895 (2011)
- A. Steinmann, B. Metzger, R. Hegenbarth, H. Giessen, in *Conference on Lasers and Electro-Optics, OSA Technical Digest (CD)* (Optical Society of America, 2011), paper CThAA5
- T. Steinle, A. Steinmann, R. Hegenbarth, H. Giessen, in preparation
- Polymicro Technologies, http://www.polymicro.com/mx_upload/superfamily/polymicro/pdfs/
- Fimmwave, http://www.photond.com/files/brochures/fimmwave_brochure
- R.H. Stolen, C. Lin, *Phys. Rev. A* **17**, 1448 (1978)
- R.H. Stolen, W.A. Reed, K.S. Kim, G.T. Harvey, *J. Lightwave Technol.* **16**, 1006 (1998)
- P.N. Kean, K. Smith, W. Sibbett, *IEE Proceedings* **134**, 163 (1987)
- M. Sheik-Bahae, A.A. Said, T.-H. Wei, D.J. Hagan, E.W. van Stryland, *IEEE J. Quantum Electron.* **26**, 760 (1990)
- S. Couris, E. Koudoumas, F. Dong, S. Leach, *J. Phys. B* **29**, 5033 (1996)